Summer 2013

Water management capabilities of bio-inspired flow field configurations for polymer electrolyte membrane fuel cells

Nicholas Warren Freer

Department:

WATER MANAGEMENT CAPABILITIES OF BIO-INSPIRED FLOW FIELD CONFIGURATIONS FOR POLYMER ELECTROLYTE MEMBRANE FUEL CELLS

by

NICHOLAS WARREN FREER

A THESIS

Presented to the Faculty of the Graduate School of the

MISSOURI UNIVERSITY OF SCIENCE AND TECHNOLOGY

In Partial Fulfillment of the Requirements for the Degree

MASTER OF SCIENCE IN MECHANICAL ENGINEERING

2013

Approved by

Umit Koylu, Advisor
Kakkattukuzhy Isaac
Xiaoming He

ABSTRACT

Fuel cells have received an increasing amount of attention over the past decade for their power production capabilities. Polymer electrolyte membrane (PEM) fuel cells in particular are researched because of their high power density, large range of operating conditions, green products, and ease of scalability. PEM fuel cells do have a number of issues that reduce their overall performance. These issues include variations in reactant distribution, materials issues for the bipolar plate, and flooding caused by poor water management. Variations in the reactant distribution causes lower overall power output due to regions of low reactant density. This means that optimizing the flow field to increase reactant density increases performance. One optimization method is to mimic natural structures that have similar functions. Leaves, lungs, and vein structures all have similar purposes to those in PEM fuel cells. Imitating their structure has been shown to improve power. It is also important to determine their water management properties. The membrane in the fuel cell must be hydrated to operate at optimally; however excess water causes mass transport issues by either blocking the channels or filling pores in the gas diffusion layer (GDL). This means that the water content in a PEM fuel cell must be delicately balanced to ensure that the membrane stays hydrated without causing flooding issues. Therefore, it is important to determine the water management capabilities of various bipolar plate designs. Clear bipolar plates are used to directly observe the water management capabilities of different flow field designs, which will be verified by the finite element model. These tests have shown that bio-inspired designs perform well in comparison with their conventional counterparts.

ACKNOWLEDGEMENTS

This project is funded by the National Science Foundation grant #CMMI-1131659.

A special thanks to Dr. Ming Leu for his invaluable advice, and help in managing the project.

Thanks to Nannan Guo for his help and guidance during this project.

TABLE OF CONTENTS

Page

LIST OF ILLUSTRATIONS

Page

LIST OF TABLES

Page

1. INTRODUCTION

Polymer electrolyte membrane (PEM) fuel cells extract power from the reaction between hydrogen and oxygen. The polymer electrolyte membrane or proton exchange membrane for which the cell is named does not allow electrons to pass through it. It does, however, allow protons to pass through. The catalyst layer is used to dissociate the hydrogen molecules from their electrons on the anode side of the cell. This allows the hydrogen to pass through the membrane and react with the oxygen on the cathode side. To finish this reaction the electrons that were previously dissociated are needed. This is how power is drawn from a PEM fuel cell. Since the electrons cannot pass through the membrane they must find a different avenue to the cathode side of the circuit. The path of least resistance is through an external circuit connected to the cell. The electron flow this external circuit in the form of current, and then finish the reaction on the cathode side of the cell. In this way PEM fuel cells draw current from the reaction between hydrogen and oxygen, with the only byproduct being water.

Bipolar plates are used to supply reactants, and to remove excess product from PEM fuel cells. Proper flow field designs will increase the evenness of reactant supply as well as increasing the water removal rate, which can lead to substantially improved performance. Flow field design is an open ended problem. There have been a plethora of proposed designs. There are, however, four conventional designs which are used frequently in industry, and therefore viable for comparison. These four designs are as follows: pin, parallel, serpentine, and interdigitated. Each of these designs has its own unique set of benefits and detriments. The pin type designs have the most uniform

reactant distribution, as well as very low pressure drop, but have very poor water management capabilities and low flow velocity. Parallel type designs also have very low pressure drop, but still have water management issues that tend to cause channel blockage. Serpentine designs tend to have better water management capabilities and flow velocity when compared with pin and parallel type designs, but at the cost of much longer flow paths, which result in uneven reactant distribution and higher pressure drop. Interdigitated designs force flow through the gas diffusion layer (GDL), which greatly improves their water removal capabilities without increasing the length of the flow paths, but results in the highest pressure drop of any of the four designs, which leads to increased parasitic power losses. For this study a serpentine design and an interdigitated design will be used for comparison because of their generally higher power output and increased water management capabilities.

Recently a great deal of study has gone into optimizing the flow field designs in the bipolar plates. Properly designed flow fields can improve performance of a fuel cell by a number of different avenues. Well-designed flow fields improve reactant concentration in the GDL, and can also improve water management properties. There are two main directions people take when trying to improve flow field design. The first is to optimize one of the conventional designs so that its pressure drop is more uniform or so that its velocity profile is as uniformly high as possible. The second avenue people take is to use a non-conventional flow field design. These non-conventional designs can come from a number of sources. Some of them are novel designs, but most of these non-conventional designs imitate nature in some form, see Figure 1.1. There are a number of natural structures such as leaves, lung alveoli, and veins that have similar purposes as the

flow field of a PEM fuel cell. These structures have already been optimized by evolution for thousands of years to use the least work, while maintaining high levels of the reactant they are distributing. There is one key difference in requirements between most natural structures and PEM fuel cells. That is the fact that almost all natural structures have evolved to be resistant to damage. For this reason there are a lot of redundancies in natural structures that are unnecessary in PEM fuel cells.

(a)  (b) 

(c) 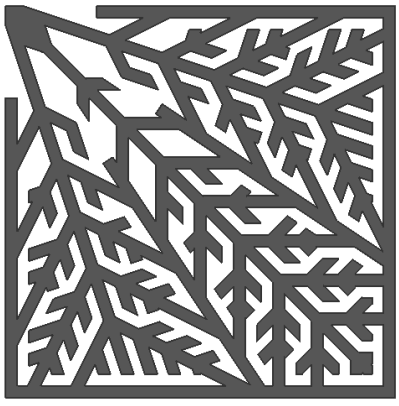 (d) 

Figure 1.1 Natural structures and their corresponding flow fields. (a) leaf veins (b) alveoli in a lung (c) flow pattern imitating a leaf (d) flow pattern imitating lung alveoli

This study will show that bio-inspired designs can increase the performance of a PEM fuel cell without significant water management issues. It will also compare two bio-inspired designs with a couple of conventional designs that are mentioned above. This will be done by analyzing simulation results, and comparing water production via direct

observation of clear bipolar plates. This is an important subject of research for a number of reasons. The first of which is that the water management capabilities of specific designs are one of the least understood properties of a PEM fuel cell configuration. Also, all previous work looked at just a single conventional design for the purpose of studying water production. This study aims to compare the water management capabilities of different flow field configurations, which has not been done in previous works. In this way, a better understanding of water management capabilities in different flow field configurations can be achieved.

The objectives of this thesis are as follows. Firstly, the water production of different flow fields is to be directly observed. These results should be used to compare the water management capabilities of different flow field designs. Finally, simulations should be used to support the experimental findings, and to explore in greater depth the reasons why specific designs have increased performance or greater water management capabilities.

2. REVIEW OF LITERATURE

Flow field design of the bipolar plate is an extremely important part of a fuel cell since proper flow field design has been shown to drastically improve fuel cell performance [33]. As such there has been considerable research done into determining what constitutes a proper flow field design. There are two main methods for attempting to improve the flow field of a bipolar plate. The first is to attempt to optimize a given geometry by modifying width, depth, or channel shape [6, 9, 15, 31, 32, 47, 49]. The second option is to modify the base geometry to try to improve performance. This is a much more difficult proposition because the problem is open-ended. Some people have attempted novel flow field designs. These would include porous flow distributors [19, 43, 44], or non-standard geometries such as spirals and fractals [25, 35, 37, 45, 48, 50]. The other main option for changing the geometry of a fuel cell is to imitate a natural structure. There are many natural structures that have similar purposes to that of the bipolar plate of a PEM fuel cell. Leaf vein structure, cardiovascular vein systems and lung alveoli all are designed to distribute a gas or liquid across a distributed area as evenly as possible. PEM fuel cell flow channels have a similar purpose; therefore many flow channel designs imitate these natural structures [1-3, 7, 10, 20, 21, 38-40]. There are a few differences between these natural structures and PEM fuel cell flow fields. The first difference is that most natural structures have more redundancy than is necessary in a fuel cell because a fuel cell does not have to recover from damage caused by external sources. The second difference is that these structures do not perform removal of excess product. Since PEM fuel cells must also remove excess water it is important to study the water management

capabilities of different flow field designs. The issues of water management and flooding have been studied [27]. There are two primary methods of observing water formation. The first uses neutron imaging [26]. This is convenient because standard fuel cells can be used, but requires special imaging equipment. The other option is to create clear bipolar plates, and directly observe the water formation [14, 18, 29, 42, 46].

3. BIO-INSPIRED DESIGNS

3.1 THEORETICAL DESIGN

Many of the non-conventional designs currently being researched are based on natural structures. This is because there are a number of natural structures that have similar purposes compared to those of PEM fuel cells. Animal and leaf vein structures, as well as mammalian lung structure all have the purpose of delivering fluids to a distributed area, and to remove excess products. These structures have developed to a state that is near optimized through the process of evolution. Therefore, structures that imitate natural ones of the same purpose should show increased performance. Natural structures do have one basic requirement that is not required for PEM fuel cells that could affect the efficiency. They have a large amount of redundancy built in to mitigate the damage caused by an injury. Since this is not a requirement of PEM fuel cells there will be differences between what is most effective for leaf veins versus the flow field of PEM fuel cells. This leads to the question: what is the most effective way to remove redundancies found in leaf veins to produce the most efficient flow field design. The first bio-inspired design in this study is purely an imitation of the leaf vein structure. The second design has the loops removed, and therefore is similar to the interdigitated design. Additionally the second design uses Murray's law for the channel dimensions. These two bio-inspired designs will be compared to two conventional designs in this study. The two conventional designs used are the interdigitated design and a multi-serpentine design. All four designs are shown below in Figure 3.1. These designs will all be made of the same materials, land to channel area, and size, which means that the flow field configuration

should be the only difference that affects performance in a meaningful way. Shown below in Figure 3.1 are the four different designs. For all future figures in this paper the design order will be the same as in Figure 3.1. Also the inlet will always be located in the top left corner, which puts the outlet in the bottom left corner of for all but the serpentine design, whose's outlet is in the bottom left corner.

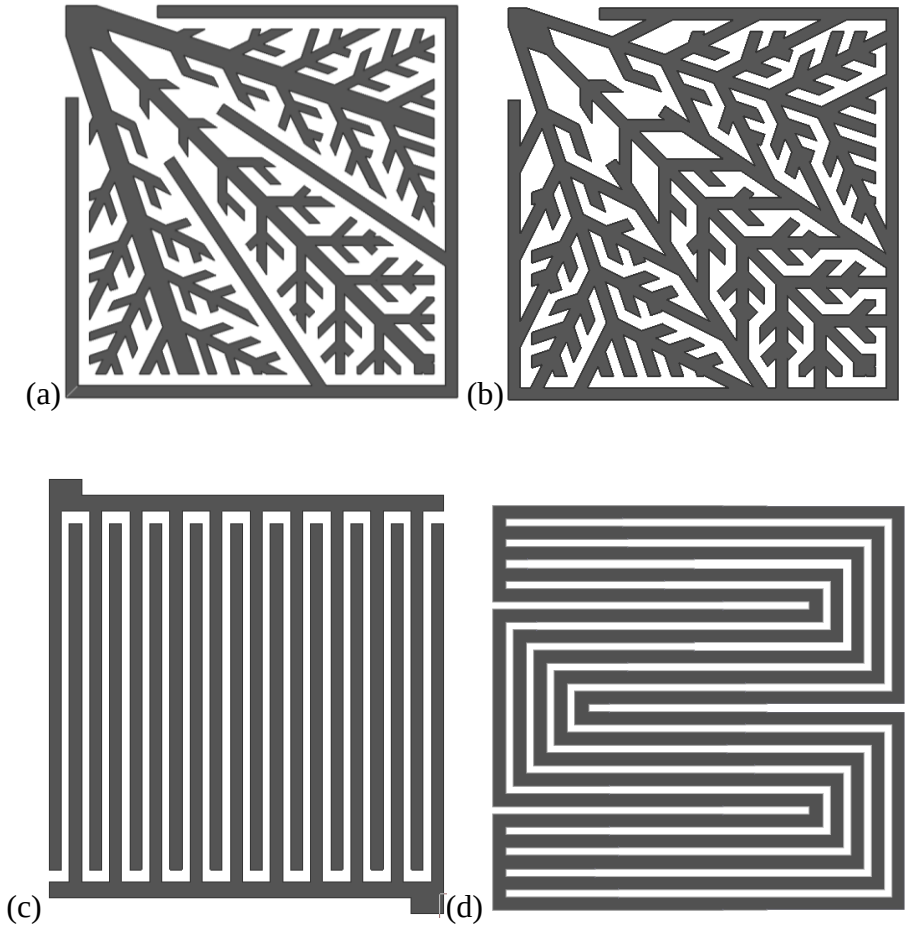

Figure 3.1 Flow field patterns, (a) Murray's law design (b) connected bioleaf design (c) interdigitated design (d) multi-serpentine design

3.2 BIPOLAR PLATE DESIGN

Bipolar plates are an extremely important component of any PEM fuel cell. Bipolar plates comprise most of the weight of a cell, as well as being the most expensive single component in the cell. As such a great deal of research has gone into optimizing both the material and the manufacturing process of bipolar plates [12, 13]. The basic requirements for any bipolar plate are as follows: flexural strength, conductivity, and corrosive resistance. The plates typically should have a flexural strength of at least 25 MPa, a conductivity of 1 kS/cm or better, and corrosion resistance of less than .016 mA/cm^2 [12]. In addition to these requirements there are also practical requirements that include minimizing cost and weight, as well as availability and machinability. For this study the requirement of transparency was also necessary so that the water formation could be directly observed. There is no known transparent material that meets all of the necessary requirements. There are no known transparent materials that have a suitably high electrical conductivity for a PEM fuel cell application. This led to the decision that a multilayer bipolar plate was necessary. The primary layer would be a transparent layer that met the strength and corrosion resistance requirements. The secondary layer would be a thin conductive layer on top of the primary layer. In this way the current could be directed through the conductive layer, and the primary layer would serve as structural support for the cell. Lexan was chosen as the primary material because of its availability and ease of machining. The second material had to be something conductive that could be thin sheets. Copper was chosen for its excellent electrical conductivity. The copper leaf was then adhered to the Lexan plate, and the channels were etched into them with a CNC

mill. This resulted in plates that had transparent backs and a conductive layer in contact with the GDL for current collection.

3.3 MURRAY'S LAW DERIVATION

Murray's Law is the natural law that defines branching in most natural distribution systems. It is based on the principle of minimum work based on the energy consumed from maintaining and transporting a given fluid [41].

Table 3.1 Nomenclature for Murray's law

Δp	Pressure drop	P_v	Viscous Power Loss per Unit Length
L	Path Length	Q	Volumetric Flow Rate
r	Path Radius	μ	Dynamic Viscosity
k_m	Metabolic Constant	P_m	Maintenance Power Loss per Unit Length
P	Power to Maintain Blood Flow	X	Branching Parameter
A_c	Cross-Sectional Area of Channel	p	Channel Perimeter
W	Channel Width	D	Channel Depth
d^H	Hydraulic Diameter	N	Number of Daughter Branches

Murray's Law assumes that there are two terms for the power required to maintain blood flow. The first of these is the energy to overcome viscous drag forces. For simplicity the transport channels are assumed to be circular, and to have fully developed laminar flow throughout. This leads to equations (1) and (2).

$$P_V = \left(\frac{\Delta p}{L}\right) Q \quad (1)$$

$$Q = \frac{\pi r^4 \Delta p}{8 \mu L} \quad (2)$$

These equations can be combined to have the viscous power loss expressed in terms of the volumetric flow rate, and the radius of the transport channels. This is done by solving

equation (2) for the pressure drop divided by the path length, and then substituting that equation into equation (1). This results in equation (3). Equation (4) is the metabolic power of maintaining blood per unit length, or the 'cost of blood volume' as referred to by Murray.

$$P_V = \frac{8\mu Q^2}{\pi r^4} \qquad (3)$$

$$P_m = k_m \pi r^2 \qquad (4)$$

If equations (3) and (4) are summed the result is the total power required to maintain blood flow through a transport system. To find the minimum power the derivative of the sum of equations (3) and (4) is taken with respect to the radius of the system. This yields equation (5), which is the minimum power consumption for a given flow rate.

$$\frac{dP}{dr} = -\frac{32\mu Q^2}{\pi r^5} + 2\pi k_m r = 0 \qquad (5)$$

When the above equation is solved for the volumetric flow rate it becomes obvious that for an optimum flow there is a specific radius for any given volumetric flow rate. This is given in equation (6). Note that every term on the right hand of the equation is a constant for a given system, except for the radius.

$$Q = \frac{\pi}{4}\sqrt{\frac{k_m}{\mu}} r^3 \qquad (6)$$

If the principle of continuity is applied to a generic branch in the system, the flow rate of the parent vessel (flow in) should be equal to the flow rate of the combined child vessels (flow out). This leads to equation (7), which can be simplified into equation (8) to determine the ratio between the radii of parent and child vessels.

$$Q_{par} = \frac{\pi}{4}\sqrt{\frac{k_m}{\mu}}r_{par}^3 = \sum_{i=1}^{N} Q_{chld,i} = \frac{\pi}{4}\sqrt{\frac{k_m}{\mu}}\sum_{i=1}^{N} r_{chld,i}^3 \quad (7)$$

$$r_{par}^3 = \sum_{i=1}^{N} r_{chld,i}^3 \quad (8)$$

If all of the child vessels are assumed to have the same radii then the equation can be further simplified to equation (9). Equation (9) also has a branching parameter included in it. The branching parameter can be used to modify the purpose of the optimization. If the branching parameter equals one, then the minimum work case is achieved. The value of the branching parameter can be adjusted for increased residence times or increased flow rates.

$$r_{par}^3 = \frac{r_{chld,i}^3}{XN} \quad (9)$$

PEM fuel cells channels are generally rectangular in shape with width and depth dimensions. To account for this the hydraulic radius is employed. This gives an equivalent radius to the given channel dimensions. The definition of hydraulic radius is given below.

$$r^H = \frac{2A_c}{P} = \frac{WD}{W+D} \quad (10)$$

4. EXPERIMENTAL

For experimental testing a Greenlight Innovations G40 series fuel cell test station was used. See Figure 4.1 below for a picture of the test station. The station has screw down attachments for fuel inlet and outlet as well as current, and clamp on meters for voltage measurement. The system has controls for reactant flow rates, cathode and anode back pressures, inlet flow temperatures, and dew points, back heating temperature, and either voltage or current set point. The station records the actual values of each of the controls, as well as both the current and voltage output of the fuel cell.

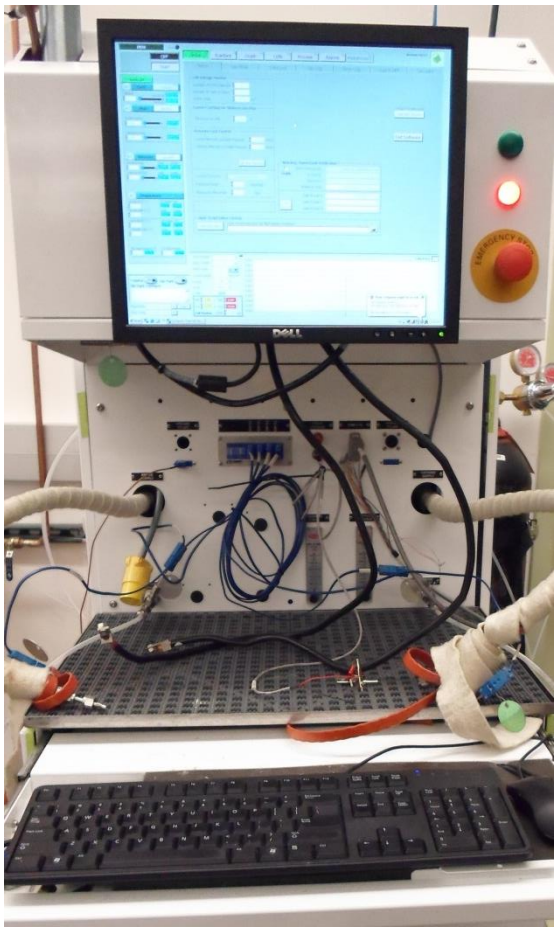

Figure 4.1 Greenlight Innovations G40 series fuel cell test station

A typical fuel cell assembly is shown below in Figure 4.2. This is the configuration that was used for the experimental verification curves shown in Figure 6.2. For the tests with clear plates the graphite plate was replaced with a clear Lexan plate with a copper layer on top. The clear plates used are shown in Figure 4.3. Figure 4.3 shows the assembled as it was tested for the direct water observation tests. The copper tabs in the top corners of Figure 4.3 were used to collect current for the tests where direct visualization was required. For the polarization tests these tabs were used to create a contact between the GDL and the current collector shown in Figure 4.2, which was made from gold plated copper. For the polarization tests the current collecting plates and end plates were used because it allowed for easier temperature regulation, and more consistent results.

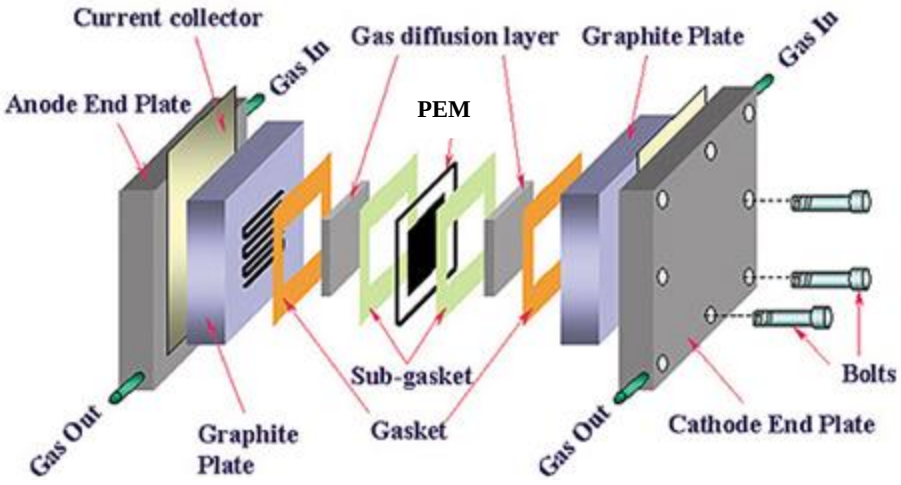

Figure 4.2 Fuel cell assembly schematic

Figure 4.3 Assembled fuel cell with clear bipolar plates

The polarization curves were obtained by setting the system to the operating conditions given in Table 5.3. After the system was set, it was allowed to reach steady state. This process took between one and two hours. Once the system has reached steady state the current density was increased in increments of 20 mA/cm^2 until the maximum current density was reached. At each new current density the system was allowed to reach a stable voltage value before moving on. This generally took less than three minutes. The polarization curve was then retaken to ensure validity.

For the long term tests the system was set to the same operating conditions as before. Then, once the system reached steady state, it was set to the maximum power density of the connected bio-leaf design. This was chosen because it was the maximum

power density that all of the designs were capable of producing. This also means that power production is not a factor in when comparing the water management capabilities of different designs. Ten minute videos were then taken at the beginning of every hour for eight hours. This allowed for determination of long term water management performance.

Table 4.1 Fuel cell dimensions

Cell width	50mm
Cell height	50mm
Bipolar Plate thickness	3mm
Channel Depth	1.5mm
GDL thickness	.3mm
Catalyst layer thickness	.01mm
Membrane thickness	.05mm

5. COMPUTATIONAL SIMULATIONS

For this study three dimensional models were created and meshed in Gambit. Fluent was then used for the computational simulations. The Gambit models used a mesh size of .5mm in both cross cell directions. For the through cell direction the mesh size was different for each section of the cell. The channel used 10 mesh elements in the through direction. The bipolar plate and GDL both used 5, and the catalyst layer and membrane each used 4. This provides a much denser mesh for the areas closer to the reaction. It also provides the least density in the bipolar plate, which doesn't need high mesh density due to the fact that there is no flow there. A variety of other mesh densities were tried, but this configuration yielded the best results. If the mesh were decreased then there were issues with accuracy, and consistency. Higher mesh densities, however, did not provide any significant improvement in accuracy, and greatly increased computational time. Computational time of a given design at a specific set point was approximately 80 minutes with this configuration.

The simulations in this study were performed using the fuel cells module of the Fluent modeling software. The following equations explain how the software determines fuel cell performance. The conservative form of the Navier-Stokes transport equation is used to solve for the fluid flow and heat transfer in the PEM fuel cell model. The generalized form of the conservative Navier-Stokes is shown in equation (11).

$$\frac{\partial}{\partial t}\int_V \rho\phi \, dV + \oint_A \rho\phi\vec{V} \cdot dA = \oint_A \Gamma_\phi \nabla\phi \cdot dA + \int_V S_\phi \, dV \quad (11)$$

This equation breaks down into five separate equations based on what is used as the transported quantity ϕ. If a constant is used as the transported quantity the equation for conservation of mass is achieved. Likewise the velocity profile is used to create the three equations for conservation of momentum. Lastly, energy per unit mass as the transport quantity results in the conservation of energy equation. The first term in equation (11) is the transient term while the second term is convective transport. The third term represents diffusion, and lastly the fourth term is a source term for any creation or removal of the source term via other methods.

Table 5.1 Nomenclature for simulations

ϕ	Transported Quantity	t	Time
A	Superficial Area	V	Volume
Γ_ϕ	Diffusivity of Transported Quantity	σ	Electrical Conductivity
φ	Electrical Potential	R	Volumetric Transfer Current
r_w	Condensation Rate	ρ	Density
s	Saturation	$\vec{V}$	Velocity Profile
k	Permeability	P_c	Capillary Pressure
ϵ	porosity	μ	Kinematic Viscosity
S_i	Source Term for Navier-Stokes	C_2	Inertial Resistance
v_i	Velocity in the i direction	v_{mag}	Velocity Magnitude
r_s	Pore Blockage Exponent	T	Temperature
D	Diffusivity	P	Pressure
R	Reaction Rate	i	Current Density
F	Faraday's Constant	R	Ideal Gas Constant
M	Mass	γ	Activity Coefficient
α	Charge Transfer Coefficient	η	Overvoltage
an	Subscript for Anode	cat	Subscript for Cathode
ref	Subscript for Reference Values	l	Subscript for Liquid Water

$$\frac{\partial(\epsilon\rho_l s)}{\partial t} + \nabla\cdot\left(\rho_l \vec{V}_l s\right) = r_w \quad (12)$$

$$\frac{\partial(\epsilon\rho_l s)}{\partial t} + \nabla\cdot\left(\rho_l \frac{Ks^3}{\mu_l}\frac{dp_c}{ds}\nabla s\right) = r_w \quad (13)$$

These two equations are used to determine the saturation based on the condensation rate and the difference between partial pressure of water and the saturation pressure. The first

equation is used for everything except the GDL. The second equation is used inside the GDL. The difference is the second term, which is a convective transport equation. The second term in equation (13) uses capillary diffusion as the main transport mechanism, which more accurately reflects conditions in the GDL.

$$\nabla \cdot (\sigma \nabla \varphi) + R = 0 \quad (14)$$

Equation (14) is the potential equation for the PEM fuel cell that is solved separately for the solid and membrane phases. This brings the total number of equations to twelve. The equations are as follows: conservation of mass, three momentum conservation equations, energy conservation, three chemical species equations (O_2, H_2, H_2O), solid and membrane phase potential, liquid saturation, and water content. These twelve equations are the basic set of equations that need to be solved to model PEM fuel cell systems.

Both the GDL and the catalyst layer are porous media. As such the model must be adjusted to reflect this reality. To account for this a negative source term is added to the momentum equations. Equation (15) is the source term to be used in the GDL and catalyst layer. The equation is proportional to the local fluid velocity, which accurately reflects viscous losses in the velocity ranges found in the GDL.

$$S_i = -(\frac{\mu}{k} v_i + C_2 \frac{1}{2} \rho v_{mag} v_i) \quad (15)$$

The diffusivity of specific species is calculated using the Stefan-Maxwell equation. The equation is designed for determining individual species diffusivities of a multi-species mixture in a porous medium. This accurately models the flow conditions of the GDL.

$$D_i = \epsilon^{1.5}(1-s)^{r_s} D_i^{ref} \left(\frac{p_{ref}}{p}\right) (\frac{T_{ref}}{T})^{1.5} \quad (16)$$

Source terms are added to the energy equations for a number of phenomena. There are terms for heat generation at the cathode catalyst layer to due chemical reaction, a term for the Joule effect, and a term for the latent heat of water for the phase change to liquid water.

Finally there are source terms added to the chemical species equations to account for the reaction taking place in the fuel cell. Hydrogen and oxygen will both receive negative sources to represent the consumption of the fuel, and water will receive a positive term for the resultant product creation. These source terms are based on the transfer current of the fuel cell. This is shown the Stefan-Maxwell equations (17a-17c).

$$S_{H_2} = -\frac{M_{w,H_2}}{2F} R_{anode} \quad (17a)$$

$$S_{O_2} = -\frac{M_{w,O_2}}{4F} R_{cathode} \quad (17b)$$

$$S_{H_2O} = -\frac{M_{w,H_2O}}{2F} R_{cathode} \quad (17c)$$

The transfer current is found using the general Butler-Volmer equations. These equations are electrochemistry models based on the oxidation and reduction rates at the catalyst surface. There is an equation for both the anode and the cathode sides of the fuel cell. Both are shown below in equations (18a) and (18b).

$$R_{an} = i_{ref}^{an} \left(\frac{[H_2]}{[H_2]_{ref}}\right)^{\gamma_{an}} \left(e^{\frac{\alpha_{an} F \eta_{an}}{RT}} - e^{\frac{-\alpha_{cat} F \eta_{an}}{RT}}\right) \quad (18a)$$

$$R_{cat} = i_{ref}^{cat} \left(\frac{[O_2]}{[O_2]_{ref}}\right)^{\gamma_{cat}} \left(e^{\frac{\alpha_{an} F \eta_{cat}}{RT}} + e^{\frac{-\alpha_{cat} F \eta_{cat}}{RT}}\right) \quad (18b)$$

Table 5.2 shows all the control values that were used for the simulations, and Table 5.3 shows the operating conditions for both the simulations as well as the experimental data.

Table 5.2 Parameters for the simulation model

Reference exchange current density at anode (A/m^2)	4.48×10^{5}
Reference exchange current density at cathode (A/m^2)	4.48
Charge transfer coefficient at anode	1.0
Charge transfer coefficient at cathode	1.0
Concentration exponent at anode	0.5
Concentration exponent at cathode	1.0
Open circuit voltage (V)	0.98
H_2 diffusivity (m^2/s)	8.0×10^{-5}
O_2 diffusivity (m^2/s)	2.0×10^{-5}
H_2O diffusivity (m^2/s)	5.0×10^{-5}
Membrane equivalent weight (kg/kmol)	1100
Catalyst layer surface-to-volume ratio (1/m)	1.25×10^{7}
GDL electric conductivity ($1/\Omega$ m)	280
GDL porosity	0.82
GDL viscous resistance at anode ($1/m^2$)	1.0×10^{12}
GDL viscous resistance at cathode ($1/m^2$)	3.86×10^{12}
GDL and catalyst layer permeability ($1/m^2$)	5.68×10^{10}
Bipolar plate electric conductivity ($1/\Omega$ m)	92600

Table 5.3 Operating conditions for PEM fuel cell simulation

Operating Temperature (K)	348
Operating Pressure (kPa)	101.3
Inlet Flow Rate (sccm)	300
Outlet Flow Rate (sccm)	1000
Relative Humidity	100%

6. RESULTS AND DISCUSSION

6.1 POLARIZATION CURVES

6.1.1 Simulated Polarization Curves. The simulation curves shown in Figure 6.1 are based on the operating conditions, and constants given in Tables 5.2 and 5.3. The given constants were determined by previous tests. See Guo et al for more information [9,15]. Figure 6.2 shows the experimental results from Guo's previous work. Since both use the same operating conditions these results can be used to verify the simulation model. The close agreement between the simulations and the experimental results in terms of both polarization curves and power density curves means that the simulations should be valid. Both show that bio-inspired designs can substantially improve performance when correctly designed. The connected bioleaf design performed poorly compared to the other designs. This is probably due to the amount of redundant channels this design has. In actual leaf structures the redundancy helps prevent against damage, but that is not an issue in PEM fuel cells. As such the extra redundancy only serves to reduce the overall flow velocity of the flow field. It also leads to regions of preferential flow and regions where there is no flow. This causes uneven reactant distribution, and areas of low reactant distribution, which lead to lower power densities and greater losses. The interdigitated design and the Murray's law design both performed quite well. This is at least in part because the inlet and outlet are not directly connected in both of these designs. When the inlet and outlet are not directly connected in the flow field it means that the reactant gasses are forced into the GDL to cross between the inlet channels and

the outlet channels. The gasses being forced into the GDL greatly increases pressure drop in the cell, but increases both the average velocity in the GDL as well as the reactant concentration in the GDL. Both of the later factors lead to better power density.

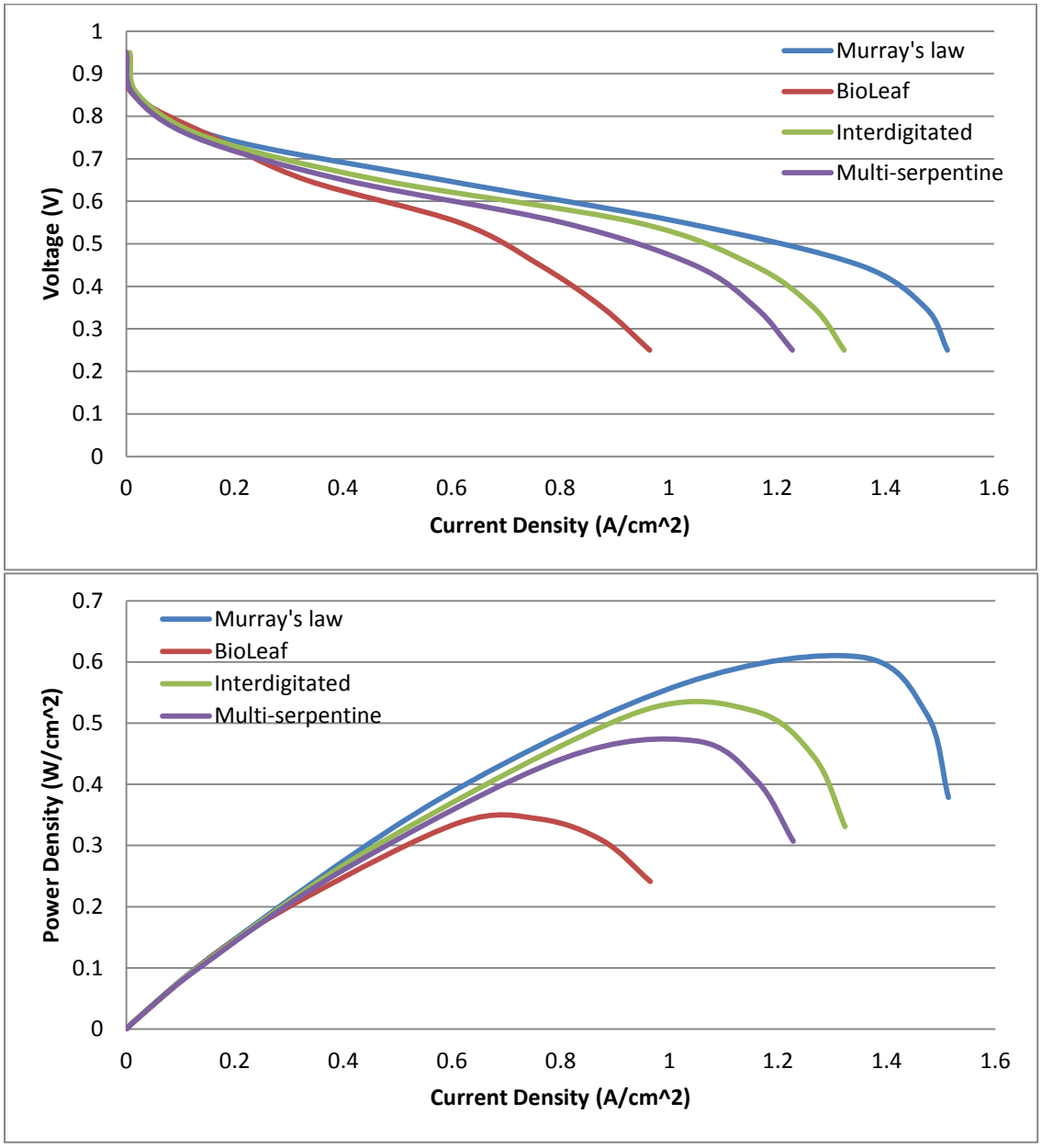

Figure 6.1 Simulated polarization and power curves for different flow field configurations

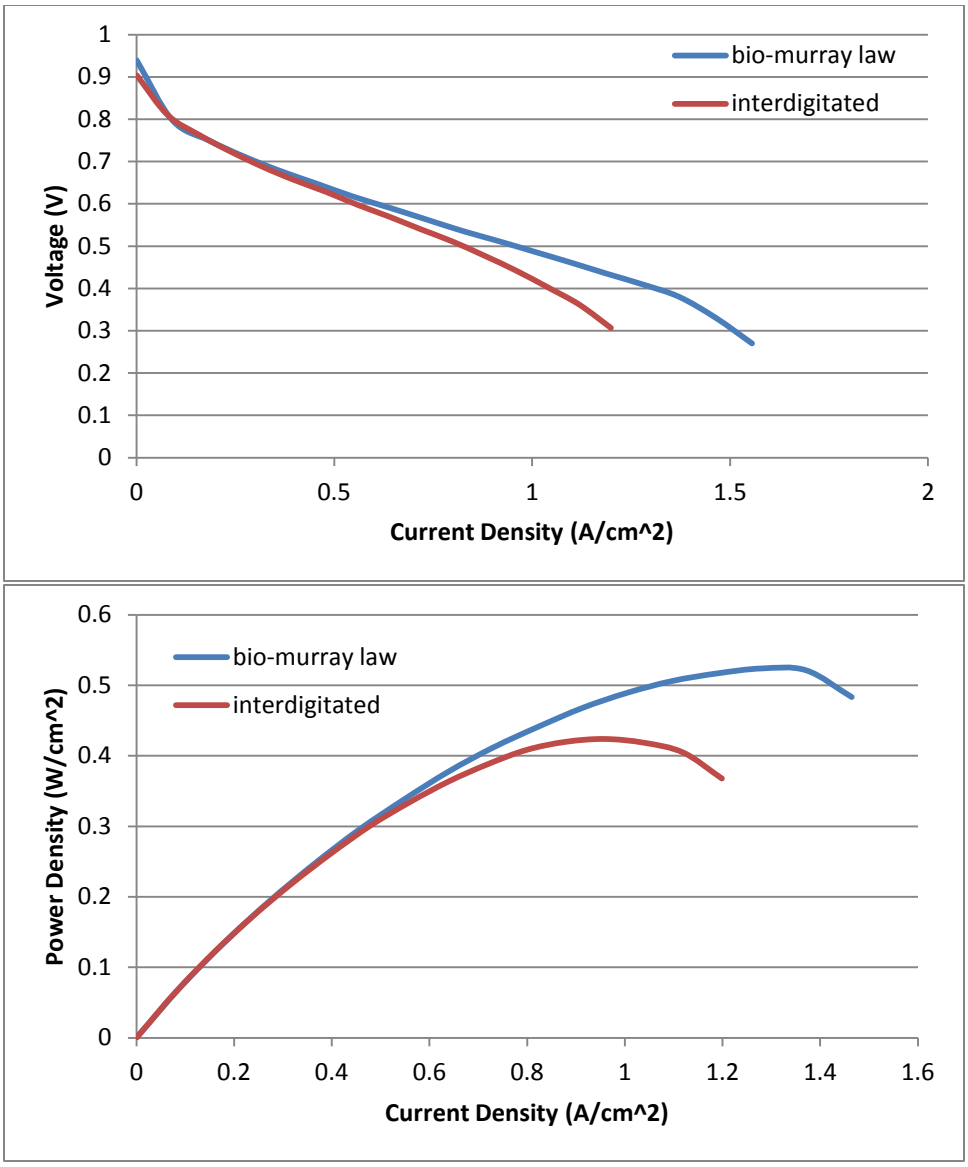

Figure 6.2 Comparison of experimental results of the bio-inspired leaf designs and conventional designs.

6.1.2 Experimental Polarization Curves. The experimental polarization curves for the clear bipolar plates are shown below. Both the polarization curve and the power curve show a similar trend as the simulation curves. The current density is not as high as would be expected from a typical fuel cell.

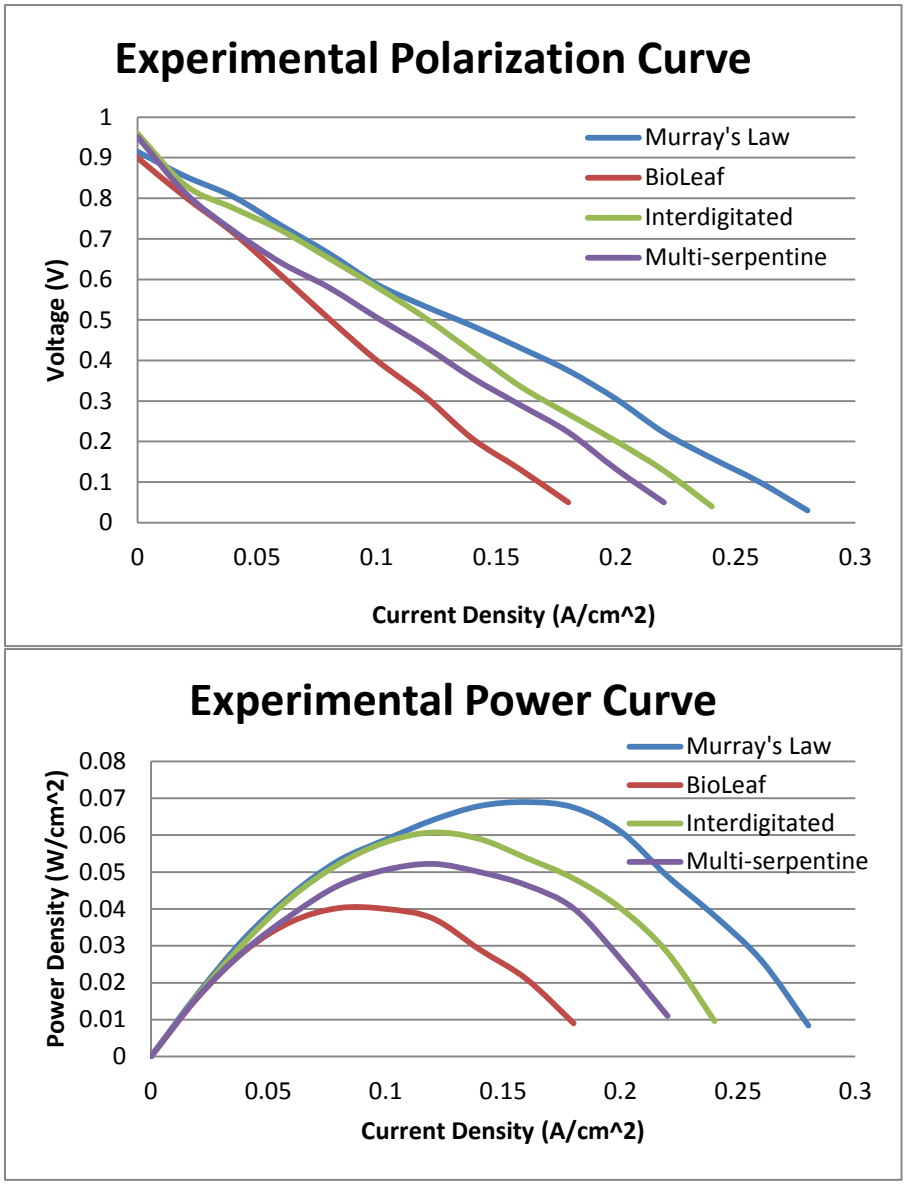

Figure 6.3 Clear bipolar plates experimental polarization and power curves

As can be seen from Figure 6.3 the current density from the clear cells is lower than would be expected. There are a couple of issues that led to this low performance. These issues are caused by the nature of the clear plates. Since there are no clear materials that meet all of the requirements for a PEM fuel cell bipolar plate a material was chosen that only lacked conductivity. For this reason the thin copper film was added between the GDL and the bipolar plate. Since these are between the GDL and the bipolar plate they must be thin or they will cause reactant leakage issues. This means that very thin wires are carrying large currents. This can cause significant losses since or signal voltage is in the range of 0-1 volts. There is also the additional issue of corrosion of the copper. Corrosion of the copper greatly increases its resistance, which leads to increased losses due to electrical resistance. The combination of these two factors accounts for the low current density seen in the experimental results with clear bipolar plates.

6.2 PRESSURE CONTOURS

The pressure distribution is an important factor in the performance of PEM fuel cells. High pressure drop across the cell increases the water management capabilities of the cell, but causes issues with reactant distribution and parasitic power losses in the cell. Therefore it is best to have the smallest pressure distribution that actually keeps the cell clear of water buildup.

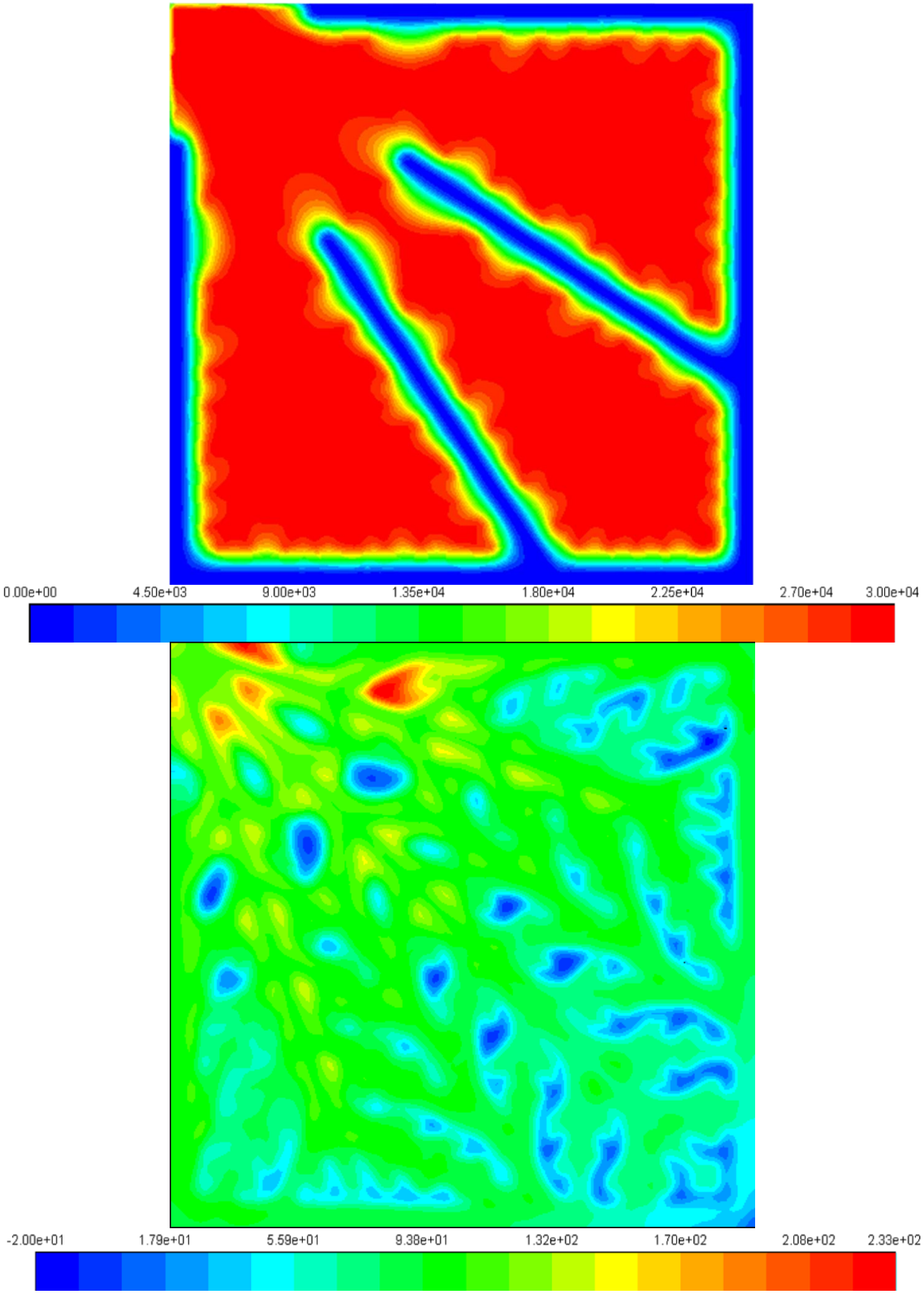

Figure 6.4 Pressure distributions for different flow fields (Pa)

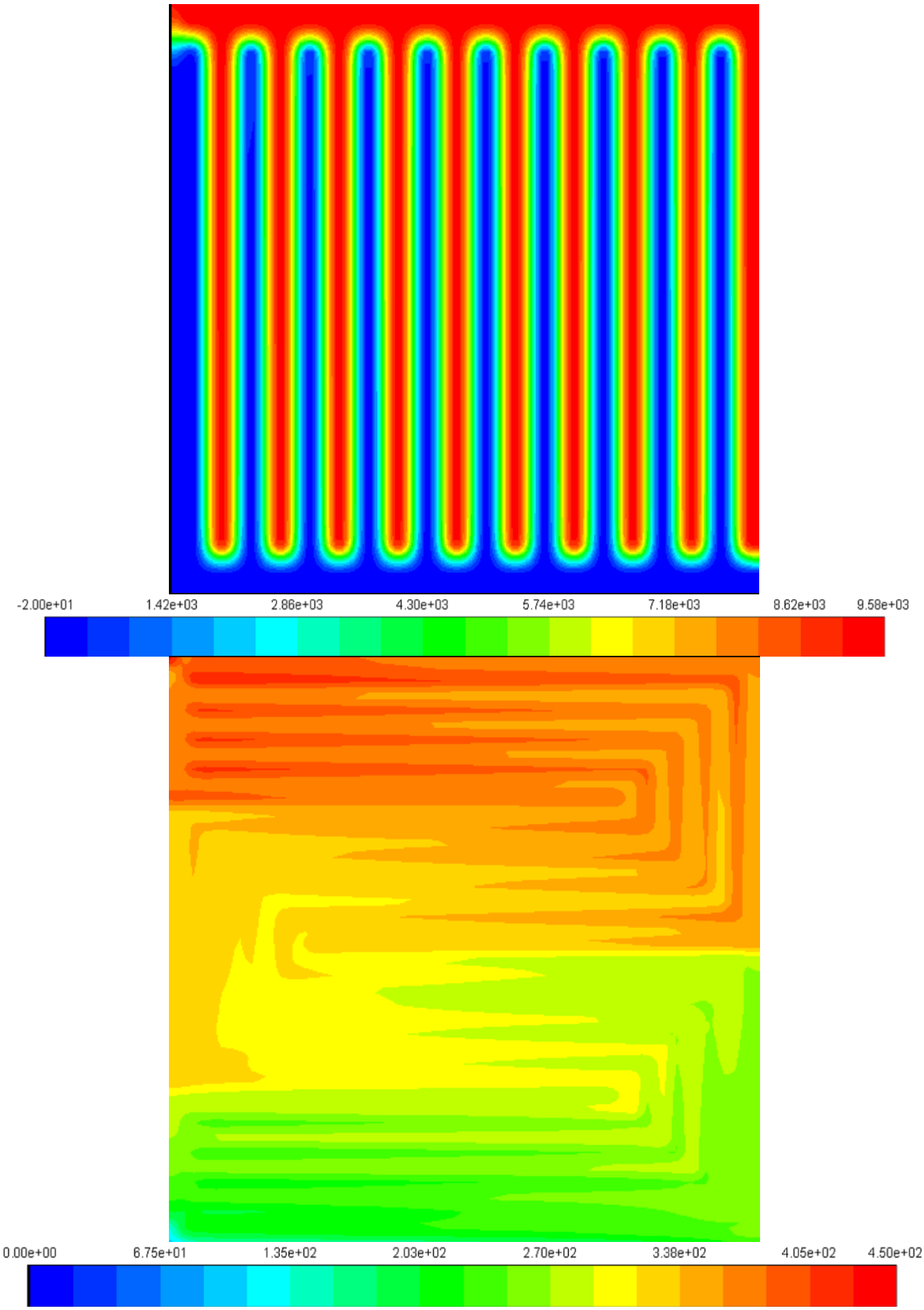

Figure 6.4 Pressure distributions for different flow fields (Pa) (cont.)

Figure 6.4 shows the static pressure of each of the different flow field designs in the GDL. It is important to note that the scalings of the pressure contours are different. The interdigitated design and the Murray's law design have the greatest pressure drop. That is the expected result because neither of these two designs have channels where the inlet and outlet are directly connected. This means that the flow is forced through the GDL, which will increase reactant density at the catalyst layer, and also improves the water management capabilities. Additional flow through the GDL means that water produced at the membrane, which moves into the GDL, will be more quickly moved into the channels, and then to the outlet. The downside here is that it requires more energy to power the inlet flows, which increases the parasitic power losses incurred by the cell. Of the other two designs, the bio-leaf design has the lowest pressure drop by a significant margin. This is an expected result due to the connected and highly redundant nature of the bio-leaf's flow channels. The high number of connections means that pressure equalizes quickly and easily. Also, the average inlet to outlet path is shortest in the bio-leaf design. Longer average path lengths increase pressure drop, which is why the serpentine design has higher pressure drop than the bio-leaf design in spite of still having a connected design.

6.3 VELOCITY CONTOURS

Even and high velocity profiles are optimal for PEM fuel cells. Higher velocities lead to a significant increase in the ability of a cell to move liquid water out of a cell, as well as reducing the time it takes to remove the produced water from the cell. Uniform velocity profiles provide a more even distribution of reactants and similar residence times of the reactants. This means that power generation across the cell is more uniform.

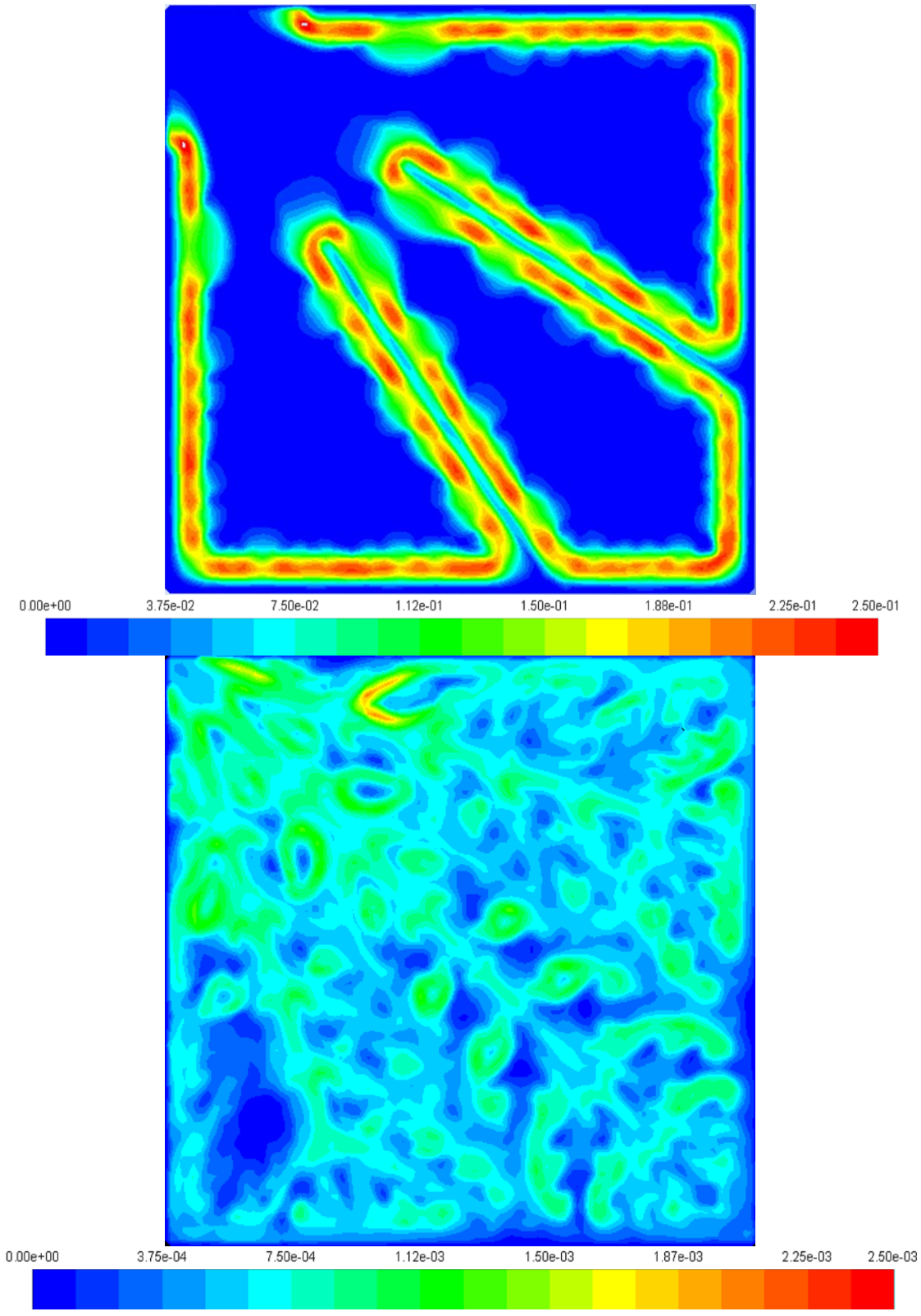

Figure 6.5 Velocity profiles for different flow field configurations (m/s)

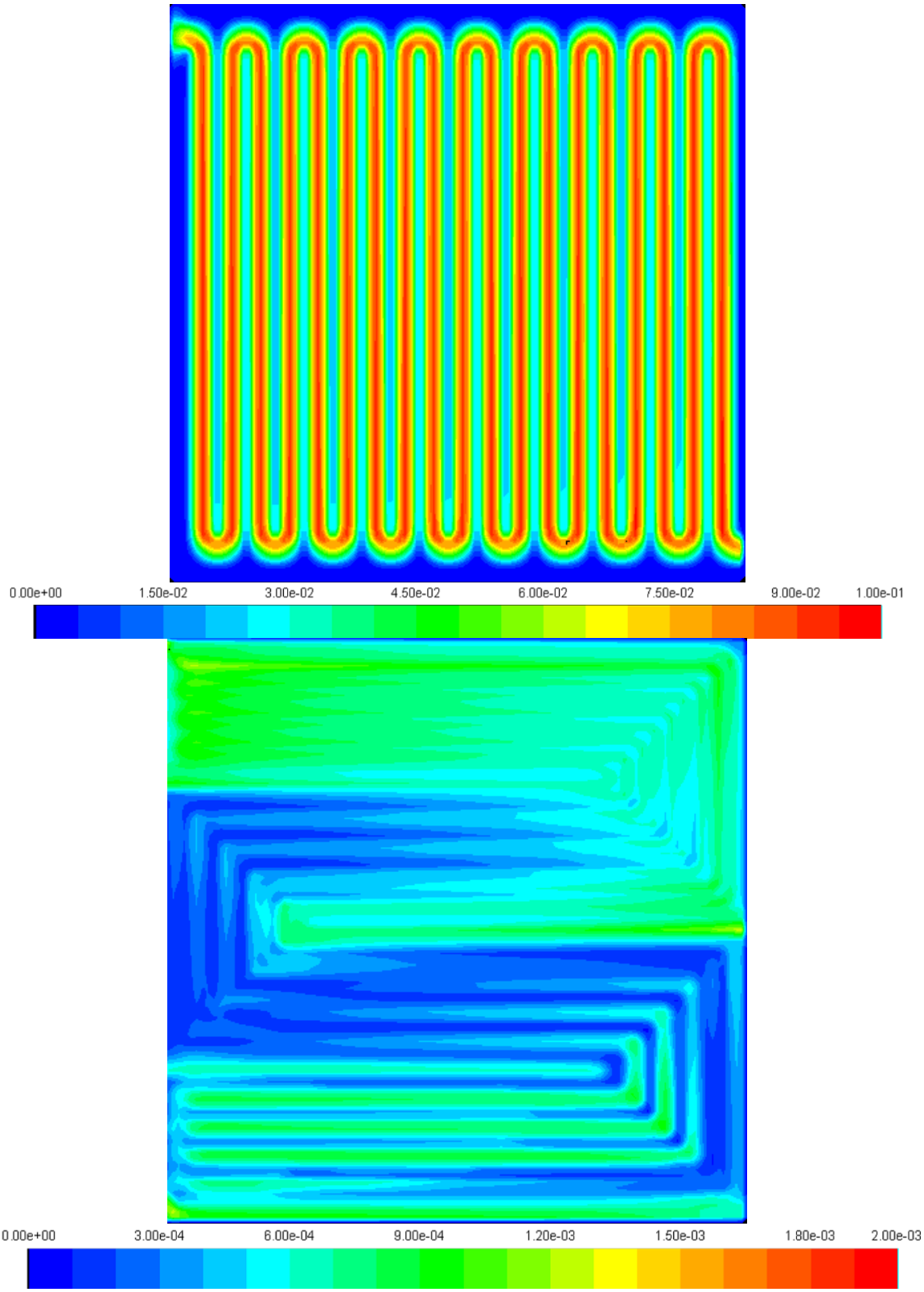

Figure 6.5 Velocity profiles for different flow field configurations (m/s) (cont.)

Velocity in the flow channels is determined more by the inlet flow rate than by channel design. The velocity in the GDL, however, is almost entirely determined by channel design. As such Figure 6.5 shows the velocity distribution of the different flow field designs. Note that the scales of the velocities are different for different designs. The two non-connected designs (interdigitated and Murray's law) have GDL velocities on the order of tenths of a meter per second, whereas the connected designs have velocities of millimeters per second. This indicates that the two non-connected designs should carry water out of the GDL much more quickly than either of the connected designs. The interdigitated design has a much more uniform velocity profile than the Murray's law design. However, the Murray's law design has higher maximum velocities. Uniform velocity profile leads to more uniform reactant distribution, and higher maximum velocities lead to faster water removal. Which of these factors is more important in terms of power density depends on whether reactant distribution or water removal is a more important factor in the fuel cell.

6.4 REACTANT MASS DISTRIBUTION

6.4.1 Hydrogen Distribution. Reactant mass fraction distributions want to follow a similar trend to the velocity profile. The higher the reactant mass fraction the better because it leads to increased reaction rate, and the uniform reactant density leads to even current density across the cell.

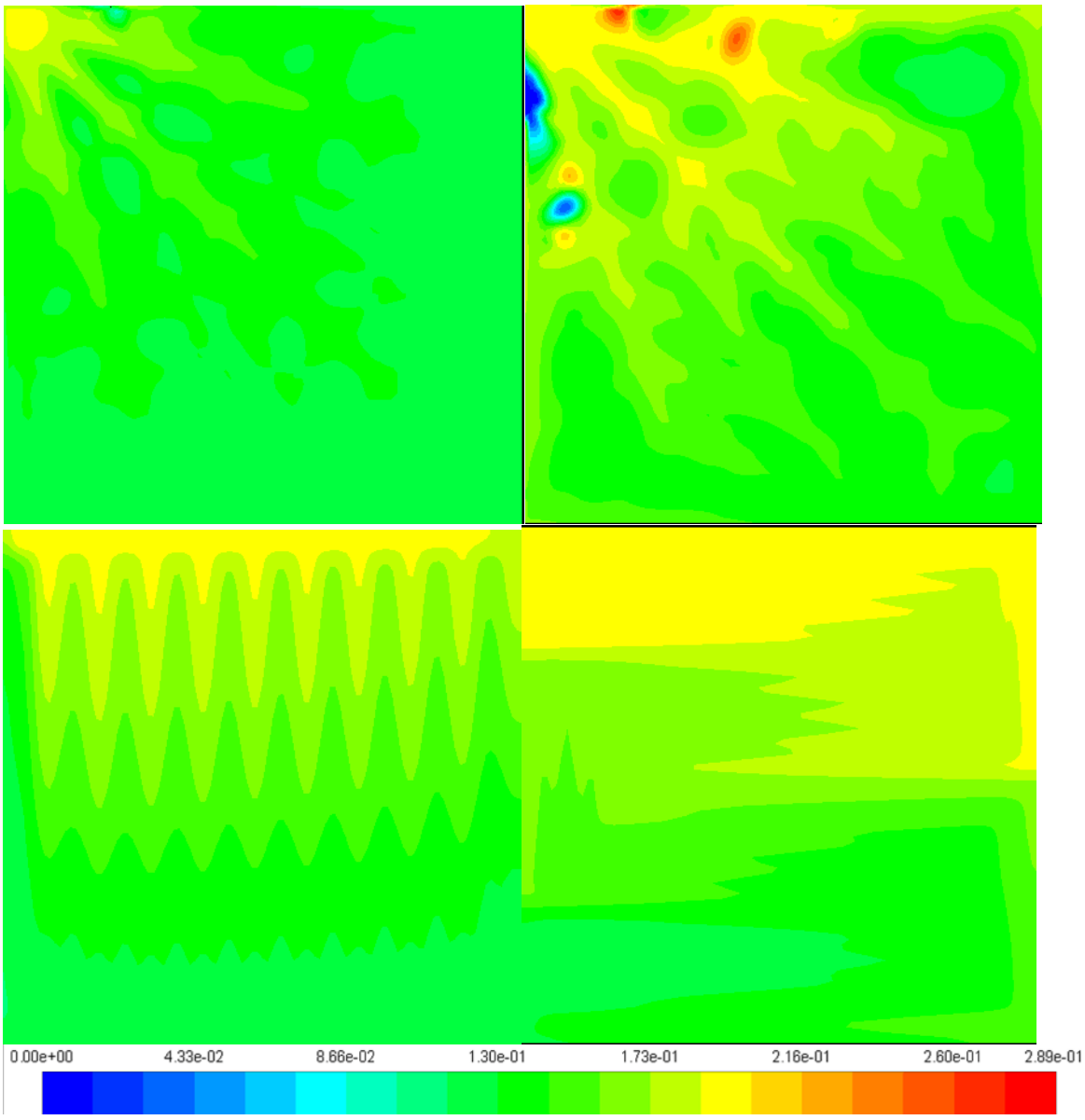

Figure 6.6 Hydrogen mass fraction distribution for different flow field designs

The hydrogen distributions for all of these designs are fairly similar. The bio-leaf design has the least uniform hydrogen distribution. There are a few small areas of both very high and very low hydrogen mass fraction. This is likely caused be high connectivity of the cell causing areas of preferential flow. A similar effect is sometimes seen in pin type designs or parallel type designs. The other three designs show fairly

similar trend of mass fractions around .2 near the inlet, and mass fractions that drop off to around .13 in the rest of the GDL. These designs all have very good uniformity over the entire cell, which means that there is not likely any issues with hydrogen distribution.

6.4.2 Oxygen Distribution. The oxygen distribution is far less uniform than that of the hydrogen. The bio-leaf design is by far the worst of these designs. The bio-leaf design has very uniform pressure, lots or redundant connections and low GDL velocity. All of these factors lead to a design where there is no significant impetus for the oxygen to move into the GDL. The uniformity of the pressure means that there is little under rib flow because the pressure is already so close to equal. This is exacerbated by the fact that all of the channels are connected, which means the path of least resistance will almost always be through the channels. This implies that the primary transport mechanism for oxygen transport into the GDL is diffusion.

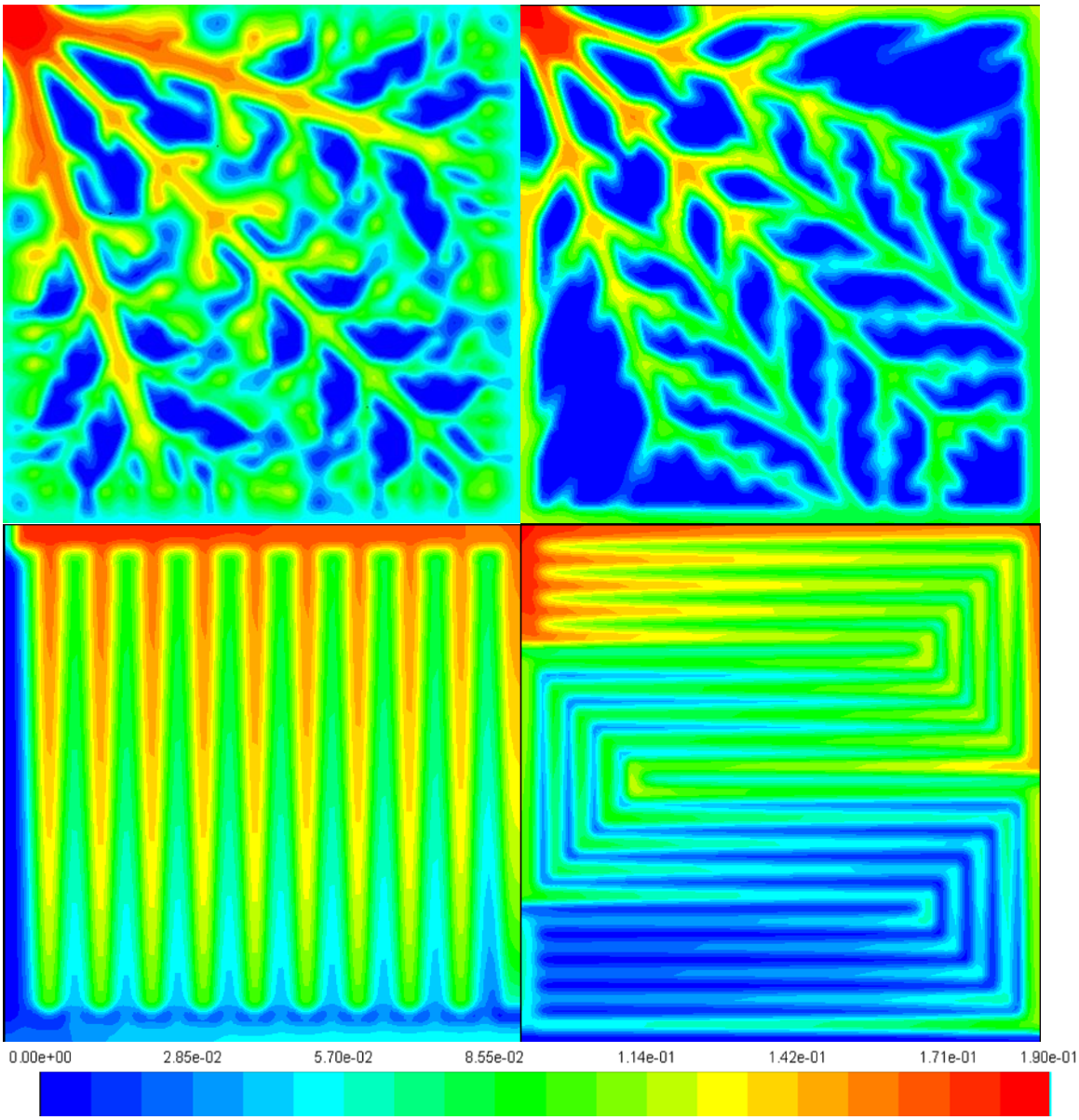

Figure 6.7 Oxygen mass density distributions for different flow fields

All of the other designs are caused primarily by forced convection due to the pressure differential, and lack of connectivity between channels. The issue with diffusion being the primary method of transport is that it is very slow, and creates areas of extremely low reactant mass fraction far away from the channels. This means that designs with too much connectivity and too low of a pressure differential will tend to have issues

with oxygen distribution, which will lower overall performance. Convective flow on the other hand causes flow under the land areas to equalize pressure. This means that there will be generally higher oxygen densities in the GDL, which leads to better performance. The serpentine design shows a marked decrease in reactant density as the flow progresses toward the outlet. This is caused by oxygen being consumed along the flow path. The longer the flow path is, the larger of an issue this becomes. This is why most designs use multiple serpentine paths rather than a single serpentine path. The two non-connected designs have better flow distributions. The interdigitated design appears to have more uniform flow distribution than the bio-inspired design in this case. This agrees with the results from the velocity section. The Murray's law design has some areas that show low oxygen density but they are significantly reduced compared to the bio-leaf design because the Murray's law's design forces flow through the GDL. This increases oxygen density in the areas away from the channels by forcing the flow to travel under the land areas to reach the outlet side of the flow field.

6.5 WATER MANAGEMENT

Water management within the fuel cell is one of the most important considerations because excess water causes flooding that reduces power. There is however a balancing act because the membrane must remain hydrated to stay conductive. If the membrane begins to dry out the conductivity will drop significantly. For this reason the inlet flows for most fuel cells are fully hydrated. This means that any water produced in the cell will cause the water vapor pressure to rise above the saturation vapor pressure, causing the formation of liquid water that must be removed from the system. Figure 6.8 show the different levels of liquid water formation.

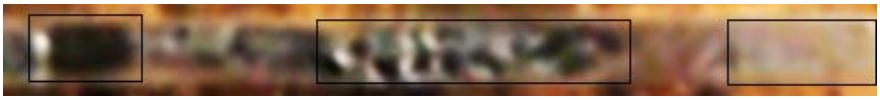

Figure 6.8 Different types of water formations

The first box shows a plug flow. Water has completely blocked the channel, and must be moved out of the channel before flow can resume. The second box is a group of slug flows. Slug flow is where liquid water has grouped together into droplets. The last box is vaporous water that is near condensing. These are the three stages that water will be found in the channels. Water vapor either moves with the reactant flow or it condenses into slugs. Slugs do not move very quickly because the flow tends to just pass around them. This being the case slugs either slowly re-evaporate or are carried off as vapor, or, more likely, they continue to grow until they reach plug flow conditions. Plug flows have the ability to evaporate just like slug flows, but since they block the channels in which they reside the flow tends to push the plug to the outlet. This causes the plug to clear taking all the liquid water with it and return to channel to a state of only water vapor and excess reactant being present, like the third box in Figure 6.8. For plug flows that are not connected to the outlet this process is more difficult. This means that the ends of channels that are not connected to the outlet are at risk to have water build up in them, and not clear quickly because to clear the blocked channel the liquid water has to be forced through the GDL to the outlet side of the flow field. The image shown in Figure 6.8 was taken from one of the middle two outlet channels of the Murray's law design. Figures 6.9 and 6.10 shown below are the water mass fraction in the GDL and in the channels. These figures show the areas in which liquid water is most likely to develop. Areas of greater water mass fraction are more likely to have liquid water develop in them.

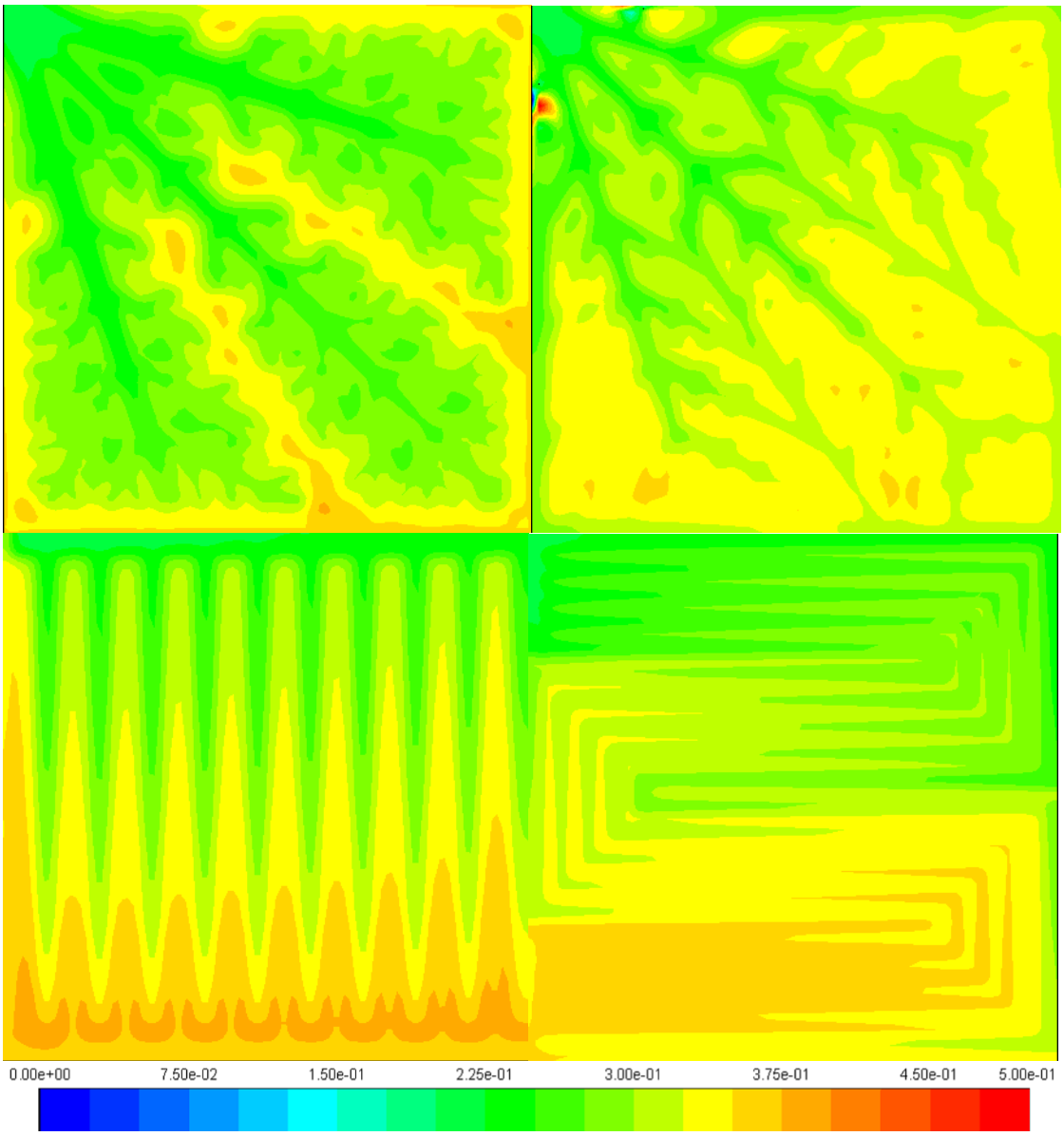

Figure 6.9 Water mass fractions for different flow field designs

The two bio-inspired designs appear to have the best water management capabilities. Especially in the GDL the bio-inspired designs have lower overall water content than the conventional designs. The connected bio-leaf has a more uniform water distribution than the Murray's law design. This is not necessarily a good thing for water management. The Murray's law has less water near the inlet channels, and more water

near the outlet channels. This means that the water in the Murray's law designs is moved more effectively towards the outlet than it is in the connected bio-leaf design. The two conventional designs appear to have most of their water located near the outlet than the inlet, which is a good sign. The conventional designs unfortunately have slightly higher average water content in the GDL.

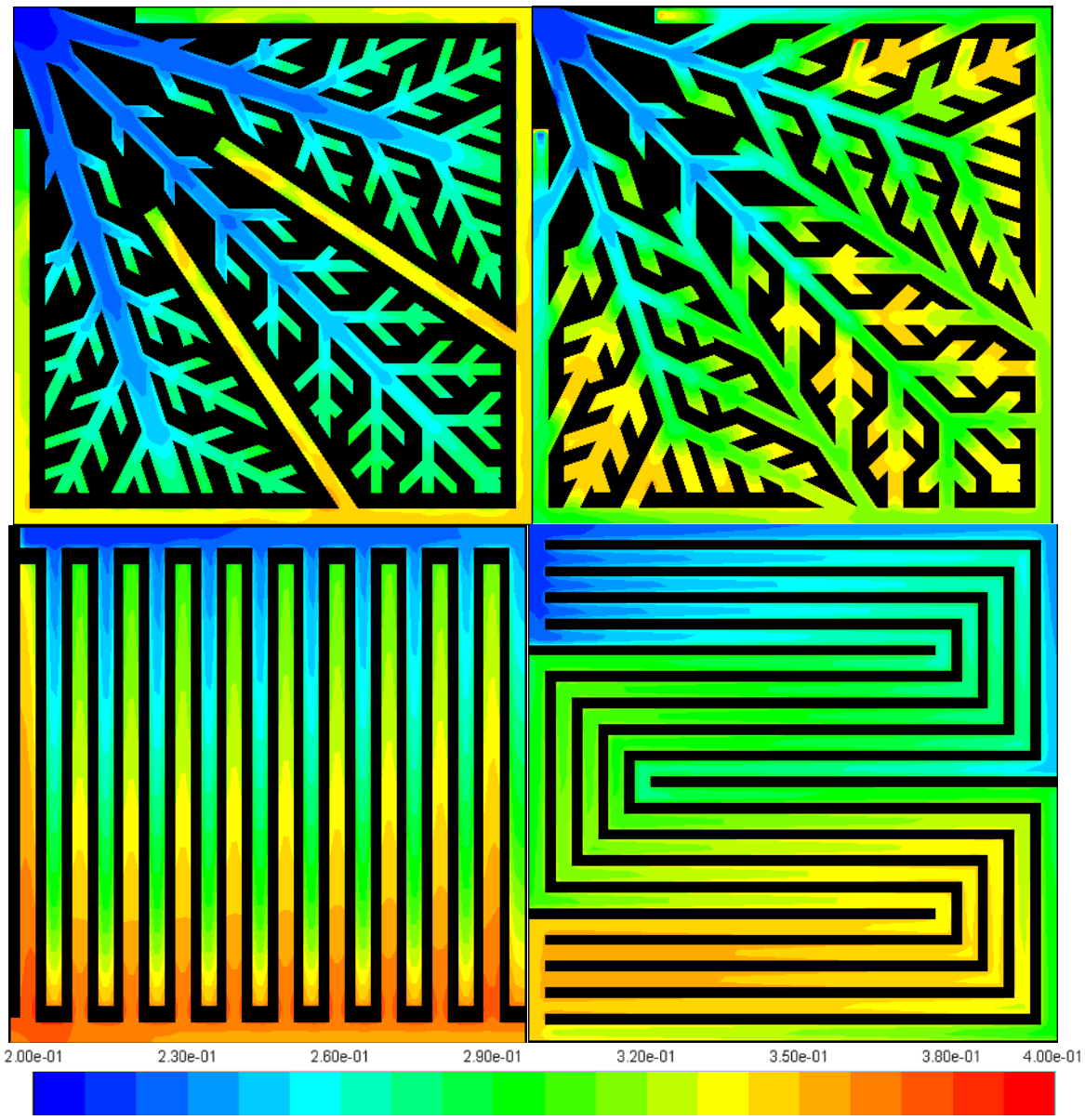

Figure 6.10 Water mass fractions in the channels for different flow field designs

The water mass fraction in the channels shows similar trends to those seen the in GDL. One major difference is that the average water content in the channels of the serpentine design is comparable to the bio-inspired designs. This suggests that the water takes a significant amount of time to move out of the GDL and into the channels. The orange and dark orange areas in Figure 6.10 are the areas where liquid water is most likely to form. For the Murray's law design Figure 6.10 indicates that most of the liquid water is formed in the outlet channels which means it will be easy to remove from the system. The connected bio-leaf design is most likely to form liquid water in the corners away from the inlet and outlet. This is not where water would be forming in an optimal case because the water must travel a significant distance to exit the cell. The serpentine design is most likely to form liquid water near the exit of the cell which is the ideal case. Finally the interdigitated design will primarily form liquid water near the outlet. There is, however, one worrying aspect: the bottom end of the inlet channels are all at risk of developing liquid water. This would mean that water would be forming on the inlet side, which could lead to a buildup of liquid water on the inlet side because the water is produced more quickly than it can be forced through the GDL.

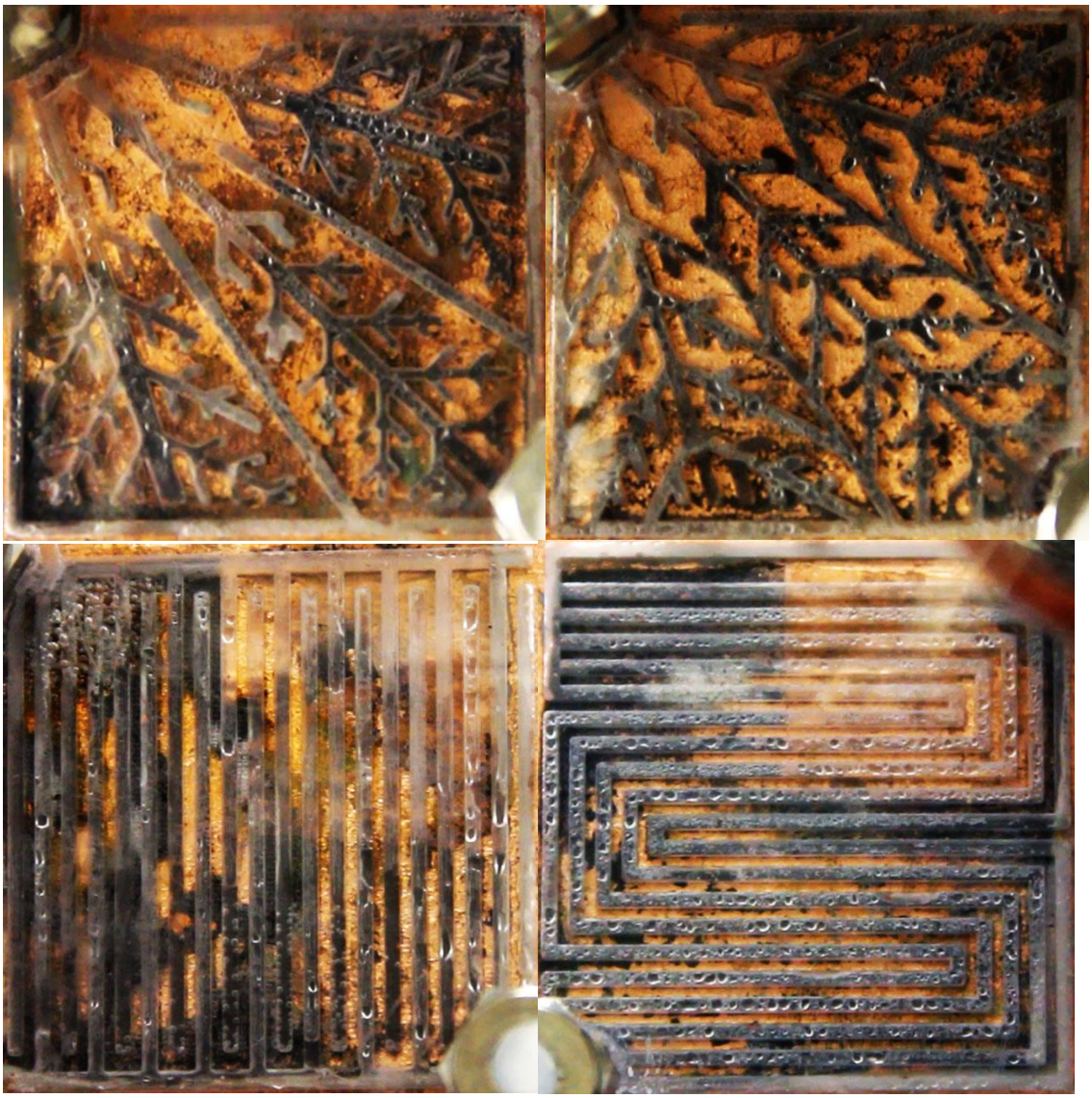

Figure 6.11 Water management photos for different flow field designs

The photos from the experiments show very similar trends to the simulation data. The conventional interdigitated design is the one that is farthest from the simulations. The experimental cell had water accumulate in the channels on the inlet side near where the channels terminate. The simulations showed that this could be an issue, but less water accumulation was obvious compared to the experimental cell. This accumulation could be caused by the lower velocities seen near channel termination, which reduces the ability

to remove liquid water from those areas. This trend is also seen in the connected bio-leaf design. There are a number of channels that terminate, and many of those channels can be seen to have some amount of liquid water accumulation. This is especially true in the regions farthest from the inlet and outlet, where the flow velocities are the lowest. The serpentine design is also showing water management capabilities similar to those shown in the simulation. The presence of water in the flow channels increases significantly as the outlet is approached. There is no slug flow in the serpentine design because of the higher average velocity. However there is still a considerable amount of water in the downstream portion of the cell, which leads to a reduction in reactant concentration, and therefore reduced performance. The interdigitated Murray's law design shows the best water management capabilities of the four designs. There is some liquid water accumulation on the inlet side of the cell, but the outlet side of the cell shows a higher density of liquid water which matches the simulation predictions. This design also shows the lowest overall level of liquid water of the four designs. These results support the hypothesis that bio-inspired designs can be used to increase the performance of a fuel cell by increasing its water management capabilities, especially when the cell is modified to remove some of the unnecessary redundancies found in all natural structures.

Table 6.1 Slug and Plug formation by flow field design

	Murray's Law		Bio-Leaf		Interdigitated		Multi-Serpentine	
	Slugs	Plugs/ Min	Slugs	Plugs/ Min	Slugs	Plugs/ Min	Slugs	Plugs/ Min
Average	78.71	1.8	108.2	2.46	95.75	2.27	109.75	2.23
Standard Deviation	12.34	0.42	9.15	0.19	19.43	0.26	12.42	0.39

Table 6.1 shows the average number of slugs in the flow as well as the average number of plugs that were formed in a given minute. The videos that were taken for the second experiment were watched and the plug formations were counted in each video. They were then averaged, and divided by the video length. The slugs were also counted at the beginning of each video and were averaged. Since liquid water in the cell lowers performance the lower these numbers are the better. With this being the case the Murray's law design can be said to have the best water management performance. It has both the lowest average number of slugs and the lowest plug creation rate. The interdigitated design has the second best average number of slugs, but has a comparable number of plugs per minute to the serpentine designs. This is because of the buildup of water at the ends of inlet channels. These areas consistently built up water because of the low velocity and high GDL water content. The connected bio-leaf design had the worse number of slugs and plug rate. This means that the low velocity and pressure drop are causing water to stay in the cell for longer and build up more significantly before being removed. It should be noted that while the design has the worst average results it is not significantly worse than either of the conventional designs. The clear best design for water management though is still the Murray's law design. It has a significantly slower plug production rate than the other designs and on average has less slugs.

7. SUMMARY AND CONCLUSIONS

In this thesis, two bio-inspired designs were presented. Both designs were inspired by leaf structures. One design used connected channels of constant width, and the other design used channels whose width varied according to Murray's law. These two designs were compared with two conventional designs. The conventional designs used were a multi-serpentine design and an interdigitated design. Each of these four designs had a clear bipolar plate made so that their water management capabilities could be directly observed. Simulations of each of these four designs were also run. The simulation results allowed for analysis of different factors that contributed to each design's ability to manage the water produced in the cell.

The clear cells had issues with power generation due to low operating temperature, and corrosion of the conductive metal layer, as well as other losses. The corrosion issue means that this type of cell would not be an effective choice for mass production. Even a more corrosive resistant metal would likely provide little benefit in terms of making a viable bipolar plate for mass production because of the high price of a conductive metal with enough corrosive resistance to function in a fuel cell. The two bio-inspired designs performed very differently. The connected bio-leaf did not perform nearly as well as initially hypothesized. This design more accurately imitates the leaf vein structures than the other bio-inspired design, which means that the flow field has a large number of connections, and redundant flow paths. In nature, this leads to a resistance to damage. In fuel cells, however, it reduces performance by creating a design that does not have sufficient pressure of velocity to adequately remove water. This is seen both in the

overall performance of the cell, and in the number of slug and plug flows observed in the cell. The Murray's law design, however, performed quite well. This design significantly reduced the number of redundant flow paths, as well as used a Murray's law to help determine optimal channel widths. The combination of these two factors resulted in this being the best of the four designs by a significant margin. The Murray's law design showed the least water in the channels both in terms of number of slugs and plugs, which likely helped to push its power production above the other designs.

This thesis looked to compare the water management capabilities of bio-inspired designs with those of conventional designs. It was found that not all bio-inspired designs have good water management capabilities, since the removal of waste products is generally handled by a different mechanism than supply in natural structures. However, when the requirement differences between natural structures and PEM fuel cells are accounted for, bio-inspired designs perform quite well in comparison with conventional designs.

BIBLIOGRAPHY

[1] Arvay A, French J, Wang J, Peng X, Kannan A. Nature inspired flow field designs for proton exchange membrane fuel cell. Int. J. Hydrogen Energy, 2013, http://dx.doi.org/10.1016/j.ijhydene.2012.12.149. February 2013.

[2] Barber R, Emerson D. Optimal Design of microfluidic networks using biologically inspired principles. Microfluid Nanofluid, 2008, 4: 179-191.

[3] Barber R, Emerson D. Biomimetic design of artificial micro-vasculatures for tissue engineering. ATLA, 2010, 38, Supplement 1: 67-79.

[4] Barreras F, Lozano A, Valino L, Marin C, Pascau A. Flow distribution in a bipolar plate of a proton exchange membrane fuel cell: experiments and numerical simulation studies. J Power Sources, 2005; 144: 54-66.

[5] Bohn S, Andreotti B, Douady S, Munzinger J, Couder Y. Constitutive property of the local organization of leaf venation networks. Physical Review E, 2002; 65: 061914.

[6] Bunmark N, Limtrakul S, Fowler M, Vatanatham T, Gostick J. Assisted water management in a PEMFC with a modified flow field and its effect on performance. Int J Hydrogen Energy, 2010; 35: 6887-6896.

[7] Chapman A, Mellor I. Development of Biomimetic™ flow field plates for PEM fuel cells. The Eighth Grove Fuel Cell Symposium London, September 24–26, 2003.

[8] Cheddie D, Munroe N. Review and comparison of approaches to proton exchange membrane fuel cell modeling. J Power Sources, 2005; 147: 72-84.

[9] Durand M, Weaire D. Optimizing transport in a homogeneous network. Physical Review E, 2004, 70: 046125-5.

[10] Emerson, D, Cieslicki, K, Gu, X, Barber, R. Biomimetic design of microfluidic manifolds based on a generalized Murray's law. Lab on a Chip, 2006, 6: 447-454.

[11] Ferng Y, Su A. A three-dimensional full – cell CFD model used to investigate the effects of different flow channel designs on PEMFC performance. Int J Hydrogen Energy, 2007; 32: 4466-4476.

[12] Guo N, Leu M. Effect of Different Graphite Materials on the Electrical Conductivity and Flexural Strength of Bipolar Plates Fabricated using Selective Laser Sintering. International Journal of Hydrogen Energy, 2012, 37: 3558-3566.

[13] Guo N, Leu M. Experimental study of polymer electrolyte membrane fuel cells using a graphite composite bipolar plate fabricated by selective laser sintering. Proceedings of International SFF Symposium, Austion, TX, 2012; 212-225.

[14] Hakenjos A, Muenter H, Wittstadt U, Hebling C. A PEM fuel cell for combined measurement of current and temperature distribution, and flow field flooding. J Power Sources, 2004; 131: 213-216.

[15] Hontanon E, Escudero M, Bautista C, Garcia-Ybarra P, Daza L. Optimization of flow-field in polymer electrolyte membrane fuel cells using computational fluid dynamics techniques. J Power Sources, 2000; 86: 363-368.

[16] Iranzo A, Munoz M, Rosa F, Pino J. Numerical model for the performance prediction of a PEM fuel cell. Model results and experimental validation. Int J Hydrogen Energy, 2010; 35: 11533-11550.

[17] Iranzo A, Munoz M, Pino J, Rosa F. Update on numerical model for the performance prediction of a PEM fuel cell. Int J Hydrogen Energy, 2011; 36: 9123-9127.

[18] Jiao K, Park J, Li X. Experimental investigations on liquid water removal from the gas diffusion layer by reactant flow in a PEM fuel cell. Applied Energy, 2010; 87: 2770-2777.

[19] Kim J, Cunningham N. Development of porous carbon foam polymer electrolyte membrane fuel cell. J Power Sources, 2010; 195: 2291-2300.

[20] Kjelstrup S, Coppens M, Pharoah J, Pfeifer P. Nature-inspired energy- and material-efficient design of a polymer electrolyte membrane fuel cell. Energy Fuels, 2010; 24: 5097-5108.

[21] Kloess J, Wang X, Liu J, Shi Z, Guessous L. Investigation of bio-inspired flow channel designs for bipolar plates in proton exchange membrane fuel cells. Journal of Power Sources, 2009, 188: 132-140.

[22] Le A, Zhou B. A general model of proton exchange membrane fuel cell. J Power Sources, 2008; 182: 197-222.

[23] Le A, Zhou B, Shiu H, Lee C, Chang W. Numerical simulation and experimental validation of liquid water behaviors in a proton exchange membrane fuel cell cathode with serpentine channels. J Power Sources, 2010; 195: 7302-7315.

[24] Lee D, Bae J. Visualization of flooding in a single and stacks by using newly-designed transparent PEMFC. Int J Hydrogen Energy, 2012; 37: 422-435.

[25] Lee K, Lee S, Park M, Chu C. The development of air-breathing proton exchange membrane fuel cell (PEMFC) with a cylindrical configuration. Int J Hydrogen Energy, 2010; 25: 11844-11854.

[26] Li X, Sabir I, Park J. A flow channel design procedure for PEM fuel cells with effective water removal. J Power Sources, 2007; 163: 933-942.

[27] Li H, Tang Y, Wang Z, Shi Z, Wu S, Song D, Zhang J, Fatih K, Zhang J, Wang H, Liu Z, Abouatallah R, Mazz A. A review of water flooding issues in the proton exchange membrane fuel cell. J Power Sources, 2008; 178: 103-117.

[28] Li X, Sabir I. Review of bipolar plates in PEM fuel cells: Flow-field designs. Int J Hydrogen Energy, 2005; 30: 359-371.

[29] Liu X, Guo H, Ye F, Ma C. Water flooding and pressure drop characteristics in flow channels of proton exchange membrane fuel cells. Electrochimica Acta, 2007; 52: 3607-3614.

[30] Lobato J, Cañizares P, Rodrigo M, Pinar J, Mena E, Úbeda D. Three-dimensional model of a 50 cm^2 high temperature PEM fuel cell. Study of the flow channel geometry influence. Int J Hydrogen Energy, 2010; 35: 5510-5520.

[31] Manso A, Marzo F, Garmendia Mujika M, Barranco J, Lorenzo A. Numerical analysis of the influence of the channel cross-section aspect ratio on the performance of a PEM fuel cell with serpentine flow field design. Int J Hydrogen Energy, 2011; 36: 6795-808.

[32] Manso A, Marzo F, Barranco J, Garikano X, Mujika M. Influence of geometric parameters of the flow fields on the performance of a PEM fuel cell. A review. Int J Hydrogen Energy, 2012; 1-32.

[33] O'hayre, R, Cha, S, Colella, W, Prinz, F. Fuel cell fundamentals. 2nd ed. John Wiley & Sons, Inc., Hoboken, New Jersey, 2009, 169-179.

[34] Painter P, Eden P, Bengtsson H-U. Pulsatile blood flow, shear force, energy dissipation and Murray's law. Theoretical Biology and Medical Modelling, 2006, 3: 31-40.

[35] Ramos-Alvarado B, Hernandez-Guerrero A, Elizalde-Blancas F, Ellis M. Constructal flow distributor as a bipolar plate for proton exchange membrane fuel cells. Int J Hydrogen Energy, 2011; 36: 12965-12976.

[36] Ramos-Alvarado B, Hernandez-Guerrero A, Juarez-Robles D, Li P. Numerical parameters of the flow fields on the performance flow distributors as flow channels for PEM fuel cells. Int J Hydrogen Energy, 2012; 37: 436-448.

[37] Robles D, Hernandez-Guerrero A, Ramos-Alvarado B, Elizalde-Blancas F, Damian-Ascencio C. Multiple concentric spirals for the flow field of a proton exchange membrane fuel cell. J Power Sources, 2011; 196: 8019-8030.

[38] Roshandel R, Arbabi F, Karimi Moghaddam G. Simulation of an innovative flow-field design based on a bio-inspired pattern for PEM fuel cells. Renewable Energy, 2012, 41: 86-95.

[39] Roshandel R, Arbabi F, Moghaddam K. Simulation of an innovative flow-field design based on a bio inspired pattern for PEM fuel cells. Renewable Energy, 2012; 41: 86-95.

[40] Senn S, Poulikakos D. Laminar mixing, heat transfer and pressure drop in tree-like microchannel nets and their application for thermal management in polymer electrolyte fuel cells. J Power Sources, 2004; 130: 178-191.

[41] Sherman T. On connecting large vessels to small: the meaning of Murray's law. The Journal of General Physiology, 1981, 78: 431-453.

[42] Spernjak D, Prasad A, Advani S. Experimental investigation of liquid water formation and transport in a transparent single-serpentine PEM fuel cell. J Power Sources, 2007; 170: 334-344.

[43] Tang Y, Yuan W, Pan M, Wan Z. Feasibility study of porous copper fiber sintered felt: a novel porous flow field in proton exchange membrane fuel cells. Int J Hydrogen Energy, 2010; 35: 9661-9667.

[44] Tsai B, Tseng C, Liu Z, Wang C, Lee C, Yang C, Lo S. Effects of flow field design on the performance of a PEm fuel cell with metal foam as the flow distributor. Int J Hydrogen Energy, 2012; 37: 13060-13066.

[45] Tüber K, Oedegaard A, Hermann M, Hebling C. Investigation of fractal flow-fields in portable proton exchange membrane and direct methanol fuel cells. Journal of Power Sources, 2004, 131: 175-181.

[46] Tüber K, Pócza D, Hebling C. Visualization of water buildup in the cathode of a transparent PEM fuel cell. J Power Sources, 2003; 124: 403-414.

[47] Wang X, Huang Y, Cheng C, Jang J, Lee D, Yan W, Su A. An inverse geometry design problem for optimization of single serpentine flow field of PEM fuel cell. Int J Hydrogen Energy, 2010; 35: 4547-4557.

[48] Wang C, Hu Y, Zheng P. Novel biometric flow slab design for improvement of PEMFC performance. Applied Energy, 2010; 87: 1366-1375.

[49] Wang X, Lu G, Duan Y, Lee D. Numerical analysis on performances of polymer electrolyte membrane fuel cells with various cathode flow channel geometries. Int J Hydrogen Energy, 2012; 1-9.

[50] Xu C, Zhao T. A new flow field design for polymer electrolyte-based fuel cells. Electrochemistry Communications, 2007; 9: 497-503.

VITA

Nicholas Warren Freer was born in, St. Louis Missouri, USA, on March 26, 1989. In 2011, he received his B.S. in Mechanical Engineering from the Missouri University of Science and Technology, Rolla, Missouri, USA. He graduated Summa cum Laude. He then began his graduate studies at the Missouri University of Science and Technology. He taught the mechanical instrumentation lab for three semesters. In August of 2013 he received his M.S. degree in Mechanical Engineering from the Missouri University of Science and Technology, Rolla, Missouri, USA.